Journal of Sustainability Science and Management
Volume 20 Number 7, July 2025: 1482-1495
eISSN: 2672-7226

MAGNETOHYDRODYNAMICS (MHD) MIXED CONVECTION OF POWER-LAW NANOFLUID IN A LID-DRIVEN CAVITY WITH TRIANGULAR SOLID IN THE PRESENCE OF HEAT GENERATION/ABSORPTION AND CHEMICAL REACTION

AMIR FARHAN MOHAMMAD ZAMRI[1], NOR RAIHAN MOHAMAD ASIMONI[1]* AND SHARIDAN SHAFIE[2]

[1]Department of Computational and Theoretical Sciences, Kulliyyah of Science, International Islamic University Malaysia, 25200 Kuantan, Pahang, Malaysia. [2]Department of Mathematical Sciences, Faculty of Science, Universiti Teknologi Malaysia, 81310 Johor Bahru, Johor, Malaysia.

**Corresponding author: raihanasimoni@iium.edu.my*
http://doi.org/10.46754/jssm.2025.07.010
Submitted: 29 July 2023 Revised: 30 November 2024 Accepted: 13 January 2025 Published: 15 July 2025

Abstract: This paper investigates laminar mixed convection heat transfer in a lid-driven cavity containing a solid triangular block at its centre. Numerical simulations of steady, two-dimensional power-law nanofluid flow, and heat transfer characteristics are performed using the finite element method via the automated solution platform Finite Element Numerical Computation Software (FEniCS). The study examined the effects of the power-law index ($0.6 \leq n \leq 1.4$), magnetic parameter ($0 \leq M \leq 4$), heat generation/absorption ($-1 \leq Q \leq 1$), and chemical reaction ($-1 \leq \kappa \leq 1$) on heat transfer performance. Results indicated that the average Nusselt number increased by 41.28% as the power-law index increased, highlighting enhanced heat transfer due to intensified inertial effects and circulation zones near the lid. Conversely, the average Nusselt number decreased by 13.05%, 54.99%, and 2.25% with increasing magnetic effect, heat generation/absorption, and chemical reaction, respectively. However, the Sherwood number increased significantly, showing respective rises of 32.63%, 20.87%, and 112.98% with increases in the power-law index, heat generation/absorption, and chemical reaction. Among the dimensionless parameters, heat generation/absorption had the most pronounced impact on the Nusselt number, whereas chemical reaction exerted the greatest influence on the Sherwood number.

Keywords: Magnetohydrodynamics (MHD), power-law nanofluid, cavity, Buongiorno, Finite Element Numerical Computation Software (FEniCS).

Introduction

Studies on mixed convective flow in a cavity on magnetohydrodynamics (MHD) have been carried out for decades due to its wide applications in industry. There are some examples of studies on MHD mixed convective flow in different types of cavities such as lid-driven cavity (Alsabery *et al*., 2020; Ali *et al*., 2022), wavy-walled cavity (Chowdhury & Alim, 2023), and square cavity (Hossen *et al*., 2019; Rashidi *et al*., 2021; Alhussain, 2022).

It has been proven that the efficiency of heat transmission may be increased using nanofluid in place of traditional fluids (Hafeez *et al*., 2021). Nanofluid has been widely employed in several fields, including cooling, fuel, electronics, and healthcare (Ali *et al*., 2021; Grzesik, 2021). There are two widely used methods for the nanofluid model, which are Buongiorno (2006) and Tiwari and Das (2007). The main focal points of Buongiorno's model are the effects of thermophoresis and Brownian motion. In contrast, Tiwari and Das model highlights the solid volume portion of nanofluid (Selimefendigil & Chamkha, 2019).

In this paper, we are interested in studying power-law Buongiorno's nanofluid in a lid-driven cavity. Power-law fluid is a non-Newtonian fluid that follows the power-law model (Bognár *et al*., 2012). The power-law model is a standard rheological model to typically quantify shear

thinning of fluids. The fluids will change into Newtonian fluids when $n = 1$ (Zhang, 2021). In Thohura *et al*. (2021), the researchers conducted a numerical simulation of mixed convective non-Newtonian fluid flow inside a skewed cavity with a moving lid. They concluded that the rate of heat transfer in the present case is sensitive to the skew-angle as well as power-law index and the maximum heat transfer occurs in the case of dilatant (shear-thickening) fluid. Inclined walls have been a topic of research in the past few decades. Ismael *et al*. (2015) demonstrated that the inclination angle of the side walls may significantly influence the Nusselt number when the Richardson number is relatively low ($Ri \leq 1$). Additionally, the relationship between the Nusselt and Richardson numbers is varied, depending on the direction of the lid's motion (Ismael *et al*., 2015). Other studies showed that the nanofluid strategy in such cavity has a noticeable augmentation of heat transfer (Nouari *et al*., 2021; Keya *et al*., 2022; Owhaib & Al-Kouz, 2022).

Nominal energy is required to initiate a chemical reaction. Thanks to this energy, the temperature of nuclear reactors may be lowered and thermal oil can also be recovered. However, as it considers the mass transfer problem, there is relatively little literature on the impact of chemical reactions in cavities. In Reddy *et al*. (2021), the authors studied the free convection MHD flow through a porous medium over an exponentially stretching surface and found that larger values of the Schmidt number and the chemical reaction parameter serve to diminish the nanoparticle concentration. Other researchers studied the mixed convection in MHD second-grade nanofluid flow through a porous medium containing nanoparticles and gyrotactic microorganisms, they found that for the constructive (or generation) chemical reaction, the mass transfer displays an increasing behaviour (Khan, 2019). In addition, Ahmad *et al*. (2021) studied the mixed convection flow, coupled with exothermic catalytic chemical reaction along a curved surface, and found the velocity profile becoming increasingly more significant when n equals to 1 due to the uniformly heated surface temperature profile and evenly distributed mass concentration.

Numerous research have used the solid triangular block inside a lid-driven cavity. For example, influence of location of the heated triangular block along the vertical centreline of cavity was examined on mixed convection characteristics (Gangawane *et al*., 2018). They found that the highest heat transfer rates can be achieved if the position of the block is at the centre. In Kumar *et al*. (2021), the researchers explored non-Newtonian power-law fluids in the mixed convection phenomenon inside a tall lid-driven cavity, with top and bottom lids moving in opposite directions. They found that with a rise in the cavity's aspect ratio, the flow pattern becomes more dispersed inside the cavity. Heat transfer enhancement is observed at a lower aspect ratio. Location of the obstacle inside the cavity plays significant role as well in the problem of heat transfer. As shown by Ismael *et al*. (2018), positioning the solid body near the mid-height of the left wall results in maximum convective heat transfer, whereas placing it at the centre of the cavity leads to minimal heat transfer. Furthermore, it is observed that the Nusselt and Sherwood numbers exhibited opposing trends depending on the location of the solid body.

A square cavity with a triangular obstacle in the centre can be utilised in heat exchangers to enhance heat transfer by disrupting fluid flow, thereby increasing turbulence and promoting improved thermal mixing (Temiloluwa *et al*., 2022). Similarly, these configurations are valuable in the study of natural convection and heat retention, providing insights for optimising thermal insulation systems in electronics, fuel cells, military equipment, medicine, nuclear reactors, spacecraft and ships.

The aforementioned papers have inspired this study's authors to conduct the present work, that is the investigation of heat generation and chemical reaction in mixed convective of Buongiorno's nanofluid for triangular block in a lid-driven cavity. We use an automated solution technique, FEniCS to solve the problem (Logg

et al., 2011; Alnæs *et al*., 2015; Desai, 2022). The problem is performed with controlling parameters, which are the power-law index (n), magnetic effect (M), chemical reaction (K), and heat generation/absorption (Q). The velocity, temperature, and concentration profiles are also analysed.

Mathematical Formulation

The laminar mixed-convective flow of power-law nanofluid in a lid-driven cavity containing inner solid triangular block incorporating Buongiorno's nanofluid model is investigated. The effects of MHD, heat generation/absorption, and chemical reaction are considered throughout this study. This study is governed by dimensional equations (1) to (4) as follows:

$$\nabla \cdot \mathbf{u} \tag{1}$$

$$\rho_f(\mathbf{u}\cdot\nabla)\mathbf{u} = -\nabla p + K\left(\frac{\boldsymbol{\varepsilon}_{ij}\boldsymbol{\varepsilon}_{ij}}{2}\right)^{\frac{n-1}{2}}\nabla\cdot\boldsymbol{\varepsilon}_{ij} - \sigma B_0^2\mathbf{u} + \Big((1-C_0)\rho_f\beta(T-T_0) - (C-C_0)(\rho_p-\rho_f)\Big)\mathbf{g} \tag{2}$$

$$\mathbf{u}\cdot\nabla T = \alpha\nabla^2 T + \gamma\left[D_B\nabla C\cdot\nabla T + \left(\frac{D_T}{T_0}\right)\nabla T\cdot\nabla T\right] + \frac{Q_0}{c_f\rho_f}(T-T_0) \tag{3}$$

$$\mathbf{u}\cdot\nabla C = D_B\nabla^2 C + \left(\frac{D_T}{T_0}\right)\nabla^2 T - \kappa_0(C-C_0) \tag{4}$$

where $\bar{u} = (\bar{u}, \bar{v})$ is the nanofluid velocity, ρ_f is the density of the nanofluid, p is the pressure, K is flow consistency index, $\varepsilon_{ij} = (\nabla\bar{u} + \nabla\bar{u}^T)$ is the strain rate tensor, n is the power-law index (it is called shear-thinning $n < 1$, shear-thickening $n > 1$ and Newtonian fluid $n = 1$), σ is the electrical conductivity of the nanofluid, B_0 is the magnetic field strength, $\bar{C}$ is the nanofluid concentration, $\bar{T}$ is the nanofluid temperature, ρ_p is the density of the nanoparticles, β is the volumetric thermal expansion coefficient, $g = (0, g_y)$ is gravity acceleration applied to the flow, $\alpha = \frac{k}{c_f\rho_f}$ with k is thermal conductivity of nanofluid, and c_f is the heat capacitance of the base fluid, $\gamma = \frac{c_p\rho_p}{c_f\rho_f}$ with c_p is the heat capacitance of the nanoparticles, D_B is the Brownian diffusion coefficient, D_T is the thermophoretic diffusion coefficient, Q_0 is the dimensional heat generation/absorption coefficient, and K_0 is the reaction rate.

After that, equations (1) to (4) are reduced into non-dimensional forms in equations (6) to (9) using dimensionless parameters in equation (5) (Buongiorno, 2006; Kefayati, 2017):

$$\mathbf{u} = \frac{\mathbf{u}}{U}, p = \frac{p}{\rho U^2}, \nabla = L\nabla, \theta = \frac{T-T_0}{T_h-T_0}, \phi = \frac{C-C_0}{C_h-C_0} \tag{5}$$

where U is the velocity of the top wall, L is the characteristic length, T_h and T_0 are nanofluid temperature with $T_h > T_0$, and C_h and C_0 are nanofluid concentration with $C_h > C_0$. The dimensionless governing equations can be written as follows:

$$\nabla\cdot\mathbf{u} = 0 \tag{6}$$

$$(\mathbf{u}\cdot\nabla)\mathbf{u} = \frac{1}{Re}\left(\frac{\boldsymbol{\varepsilon}_{ij}\boldsymbol{\varepsilon}_{ij}}{2}\right)^{\frac{n-1}{2}}\nabla\cdot\boldsymbol{\varepsilon}_{ij} - \nabla p - M\mathbf{u} + Ri(\theta - Nr\phi)\mathbf{e_g} \tag{7}$$

$$\mathbf{u} \cdot \nabla\theta = \frac{1}{RePr}[\nabla^2\theta + Nb\nabla\phi \cdot \nabla\theta + Nt\nabla\theta \cdot \nabla\theta + Q\theta] \tag{8}$$

$$\mathbf{u} \cdot \nabla\phi = \frac{1}{RePr}\left[\frac{1}{Le}\nabla^2\phi + \frac{1}{Le}\frac{Nt}{Nb}\nabla^2\theta - \kappa\phi\right] \tag{9}$$

with corresponding dimensionless parameters defined in Kefayati (2017) in equation (10):

$$\begin{aligned} &Re = \frac{\rho_f U^{2-n} L^n}{K}, Pr = \frac{K}{\rho_f \alpha U^{1-n} L^{n-1}}, \\ &Ri = \frac{L}{U^2}(1 - C_0)\beta g(T_h - T_0), Le = \frac{\alpha}{D_B} \\ &Nb = \frac{\gamma D_B(C_h - C_0)}{\alpha}, Nt = \frac{\gamma D_T(T_h - T_0)}{T_0\alpha}, Nr = \frac{(\rho_p - \rho_f)(C_h - C_0)}{\rho_f(1 - C_0)\beta(T_h - T_0)}, \\ &M = \frac{\sigma B_0^2 L}{\rho_f U}, \kappa = \frac{L^2}{\alpha}\kappa_0, Q = \frac{Q_0 L^2}{c\rho_f \alpha} \end{aligned} \tag{10}$$

where *Re* is Reynolds number, *Pr* is Prandtl number, *Ri* is Richardson number, *Le* is Lewis number, *Nb* is Brownian diffusion parameter, *Nt* is thermophoresis parameter, *Nr* is buoyancy parameter, *M* is magnetic parameter, *K* is chemical reaction parameter, and *Q* is heat generation/absorption parameter.

Flow configuration in lid-driven cavity is shown in Figure 1. The upper wall is moving with condition of high temperature and concentration. Meanwhile, other walls are stationary with no slip condition. Vertical walls are adiabatic and bottom wall is having low temperature and concentration. The triangular block is considered a non-conducting block.

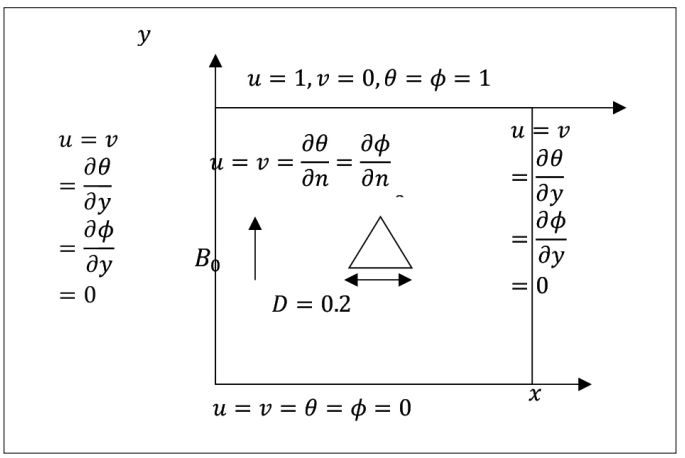

Figure 1: Flow configuration with Ω = [0, 1] x [0, 1]

The dimensionless governing equations (6) to (9) are subjected to initial and boundary conditions in equation 11.

$$\begin{aligned}
&u = 0, v = 0, \frac{\partial \phi}{\partial n} = 0, \frac{\partial \theta}{\partial n} = 0 && \text{for solid block with size } D = 0.2 \\
&u = 0, v = 0, \frac{\partial \phi}{\partial y} = 0, \frac{\partial \theta}{\partial y} = 0 && \text{for } x = 0, 0 \le y \le 1 \\
&u = 0, v = 0, \frac{\partial \phi}{\partial y} = 0, \frac{\partial \theta}{\partial y} = 0 && \text{for } x = 1, 0 \le y \le 1 \\
&u = 0, v = 0, \phi = 0, \theta = 0 && \text{for } y = 0, 0 \le x \le 1 \\
&u = 1, v = 0, \phi = 1, \theta = 1 && \text{for } y = 1, 0 \le x \le 1
\end{aligned} \tag{11}$$

where u is horizontal velocity, v is vertical velocity, ϕ is fluid concentration, θ is fluid temperature, $\frac{\partial}{\partial n}$ is normal derivative with n is the unit outward normal of the surface of the block, x is horizontal axis, and y is vertical axis.

In order to solve the problem, the FEniCS automated solution technique with finite element method is used. Weak formulation is constructed by multiplying equation (6) to (9) with test functions and integrating the equations over the domain Ω as presented in equations (12) to (15). The platform Jupyter Notebook is used to write and execute the Python code. The results of velocity, temperature, and concentration profiles are plotted using matplotlib.

$$\int_{\Omega} (\nabla \cdot u)\, q dx = 0 \tag{12}$$

$$\int_{\Omega} (\mathbf{u} \cdot \nabla)\mathbf{u} \cdot \mathbf{v} + \frac{1}{Re}\left(\frac{\boldsymbol{\varepsilon}_{ij}\boldsymbol{\varepsilon}_{ij}}{2}\right)^{\frac{n-1}{2}} \boldsymbol{\varepsilon}_{ij} \cdot \nabla \mathbf{v} - p(\nabla \cdot \mathbf{v}) + M\mathbf{u} \cdot \mathbf{v} - Ri\theta \mathbf{e_g} \cdot \mathbf{v} + RiNr\phi \mathbf{e_g} \cdot \mathbf{v}\, dx = 0 \tag{13}$$

$$\int_{\Omega} (\mathbf{u} \cdot \nabla\theta)s + \frac{1}{RePr}[\nabla\theta \cdot \nabla s - Nb(\nabla\phi \cdot \nabla\theta)s - Nt(\nabla\theta \cdot \nabla\theta)s - (Q\theta)s]\, dx = 0 \tag{14}$$

$$\int_{\Omega} (\mathbf{u} \cdot \nabla\phi)r - \frac{1}{RePr}\left[-\frac{1}{Le}\nabla\phi \cdot \nabla r - \frac{1}{Le}\frac{Nt}{Nb}(\nabla\theta \cdot \nabla r) - (\kappa\phi)r\right] dx = 0 \tag{15}$$

Results and Discussion

Numerical result has been validated in the case of Newtonian fluid (n = 1, $Nr = Nb = Nt$ = 0) without the effects of a magnetic field, heat generation/absorption, and chemical reaction ($M = Q = K$ = 0) (Iwatsu *et al*., 1993). The average Nusselt number (Nu) in this study is found to be in good agreement with the previous paper, as shown in Table 1.

Next, grid independence test is executed for mesh 64 x 64, 128 x 128, and 256 x 256 and compared with Iwatsu *et al*. (1993) with fixed parameters Re = 400, Pr = 0.71, Gr = 100. As a result, mesh 128 x 128 grid size is chosen to execute all the results in this study as it shows good agreement (Table 2).

Table 1: Comparison of average Nusselt number (*Nu*) between this study and a previous paper

Gr	*Re*	Iwatsu *et al.* (1993)	Present
10^2	100	1.94	2.0316
	400	3.84	4.0698
10^4	100	1.34	1.3946
	400	3.62	3.8231
10^6	100	1.02	1.0206
	400	1.22	1.1854

Table 2: Comparison of minimum and maximum velocity results at the cavity midsection

	Iwatsu *et al.* (1993)	Mesh 64 x 64	Mesh 128 x 128	Mesh 256 x 256
U_{min}	-0.31979227	-0.31240046	-0.32049163	-0.32455064
U_{max}	1.00000000	1.00000000	1.00000000	1.00000000
V_{min}	-0.44589245	-0.43347341	-0.44355232	-0.44875806
V_{max}	0.29554427	0.28733576	0.29548602	0.29958231

The problem is performed with controlling parameters, which are power-law indexes (n = 0.6, 0.8, 1.0, 1.2, and 1.4), magnetic effects (M = 0, 1, 2, 3, and 4), chemical reactions (K = -1, -0.5, 0, 0.5, and 1), heat generation/absorption (Q = -1, -0.5, 0, 0.5, and 1), and fixed parameters (Pr = 1, Ri = 1, Re = 100, D = 0.2, $Nb = Nt = Nr$ = 0.1, and Le = 5).

Figures 2 (a) to (c) show the effects of power-law index on v-velocity, temperature, and concentration profiles throughout the x axis at y = 0.6 and $M = Q = K$ =1. Three types of nanofluid are discussed, namely shear-thinning (n = 0.6 and 0.8), Newtonian (n = 1), and shear-thickening (n = 1.2 and 1.4) nanofluid. Negative sign of magnitude velocity shows opposite direction of vertical velocity as in Figure 2 (a). It presents that increasing n enhances the magnitude of nanofluid velocity. It is noticed in Figure 3 (a) that the red region near the top-moving wall has thickened, showing high fluid velocity as the nanofluid becomes the shear-thickening type (n = 1.4). Enhancing fluid velocity helps both heat and mass transfer, represented by the red region. Both hot and highly concentrated fluid will increase at the upper right side of cavity as indicated in Figures 3 (b) and (c). It may be seen in Figures 2 (b) and (c) that both temperature and concentration are rising. Table 3 reveals a consistent increase in both *Nu* and Sherwood number (*Sh*) as n increases from 0.6 to 1.4 (from shear-thinning to shear-thickening type). *Nu*, representing heat transfer efficiency, also rises from 0.5796 at n = 0.6 to 0.9869 at n = 1.4, indicating enhanced thermal performance with higher power-law index. Similarly, *Sh*, reflecting mass transfer efficiency, rises from 4.1277 to 6.1272 across the same range, suggesting improved mass transfer rates. This trend implies that fluids with higher power-law indices (shear-thickening nanofluid) will exhibit better heat and mass transfer characteristics, likely due to changes in flow and transport properties associated with non-Newtonian behaviour.

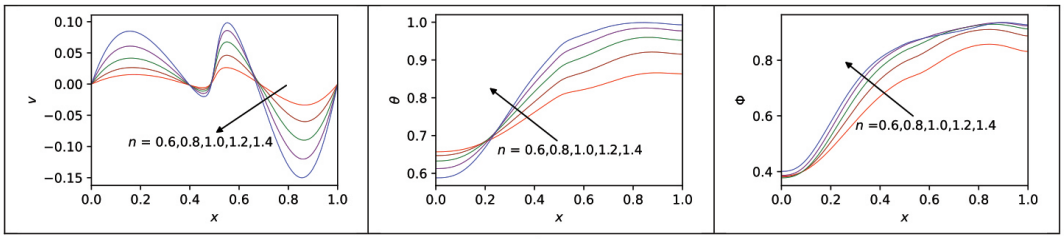

Figure 2: Variation of power-law index (n) on (a) velocity, (b) temperature, and (c) concentration profiles at $y = 0.6$

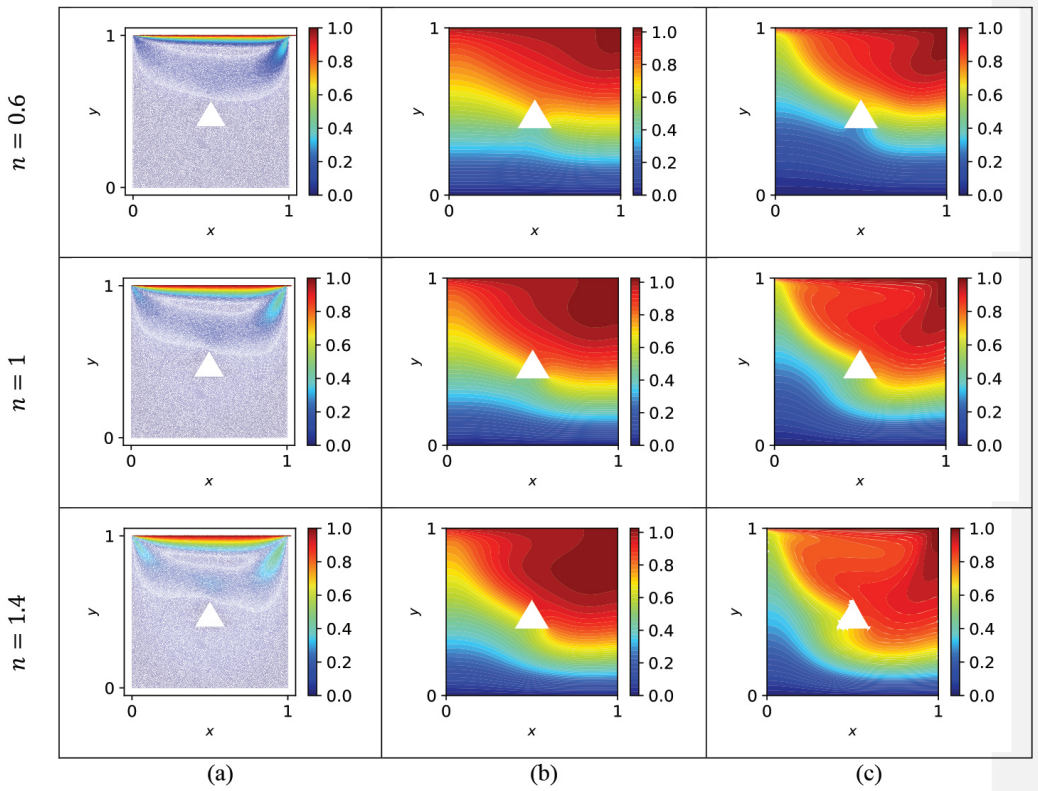

Figure 3: Variation of power-law index (n) on (a) velocity, (b) temperature, and (c) concentration profiles in the cavity

Table 3: Comparison of Nusselt number and Sherwood number for $0.6 \leq n \leq 1.4$

n	**Nusselt Number (*Nu*)**	**Sherwood Number (*Sh*)**
0.6	0.5795863	4.1277337
0.8	0.6443176	4.5981556
1.0	0.7290070	5.1133394
1.2	0.8404221	5.6295587
1.4	0.9869515	6.1272283

The influence of magnetic parameter (M) on the vertical v-velocity, temperature, and concentration profiles throughout the x-axis at y = 0.6 with Q = K = 1 and n = 0.8 is presented in Figures 4 (a) to (c). Figure 4 (a) shows that adding the value M may decrease the magnitude of velocity as the Lorentz force slows down the fluid motion. Referring to Figure 5 (a), when M = 0, high velocity is represented by the green region at the moving top wall. However, fluid velocity will show a declining pattern when M = 4. In addition, temperature and concentration profiles will also deteriorate at y = 0.6 as seen in Figures 4 (b) and (c).

Since the velocity has slowed down, both profiles have declined at the upper right of the cavity as indicated in the red regions of Figures 5 (b) and (c). Table 4 reveals that as M increases from 0 to 4, the Nu decreases from 0.6832 to 0.5940, indicating a reduction in heat transfer efficiency. Simultaneously, Sh also decreases from 4.6301 to 4.3641, reflecting a decline in mass transfer efficiency. This trend suggests that increasing M introduces a damping effect on the fluid flow, likely due to the Lorentz force, which suppresses convective heat and mass transfer mechanisms. Consequently, both thermal and concentration gradients are less effectively maintained at higher M values.

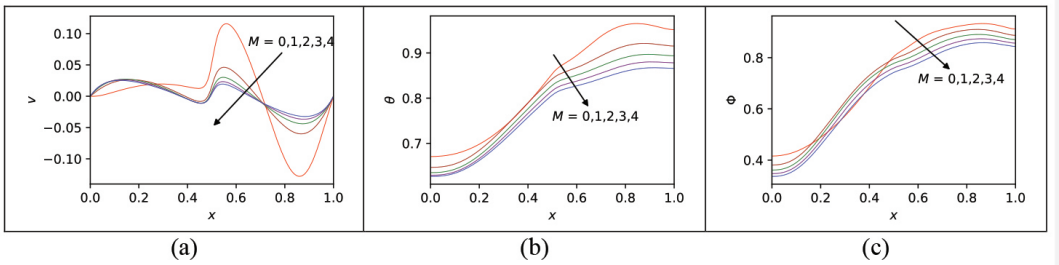

Figure 4: Variation of magnetic parameter (M) on (a) velocity, (b) temperature, and (c) concentration profiles at y = 0.6

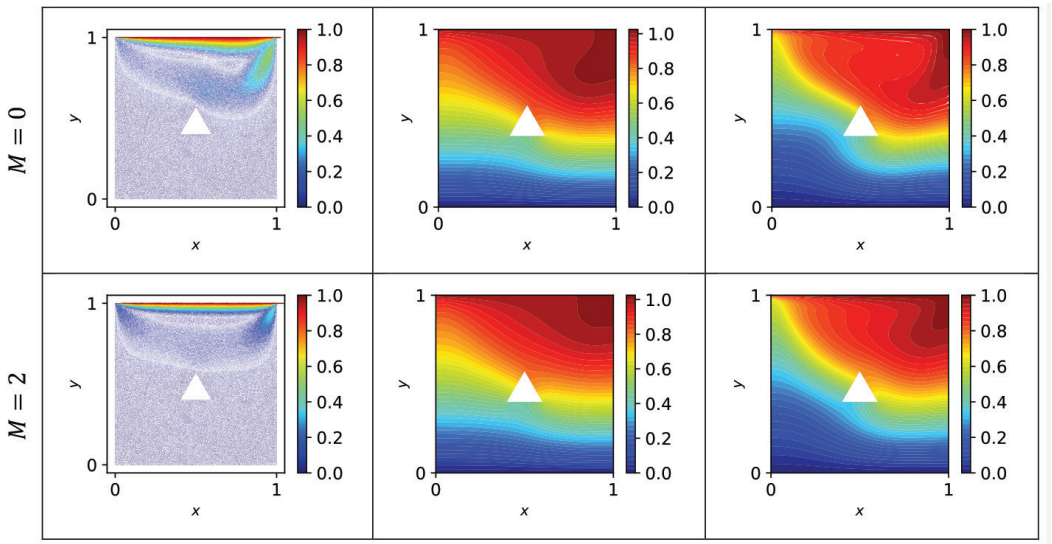

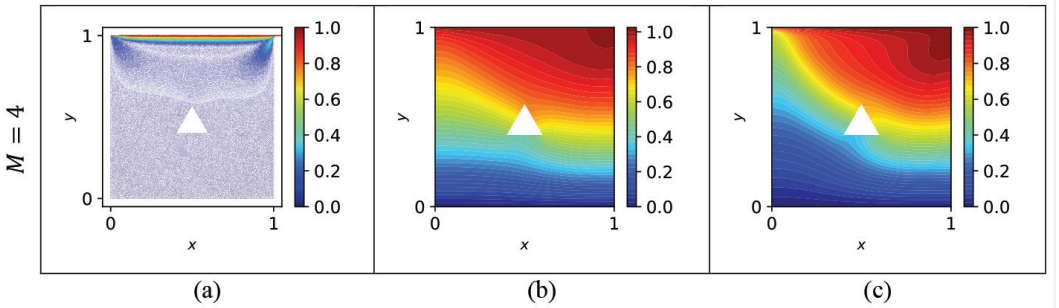

Figure 5: Variation of magnetic parameter (M) on (a) velocity, (b) temperature, and (c) concentration profiles in the cavity

Table 4: Comparison of Nusselt number and Sherwood number for $0 \leq M \leq 4$

M	Nusselt Number (Nu)	Sherwood Number (Sh)
0	0.6832195	4.6300810
1	0.6443176	4.5981556
2	0.6229701	4.5316974
3	0.6067881	4.4481203
4	0.5940255	4.3641372

The profiles of v-velocity, temperature, and concentration for various values of heat generation/absorption parameter with $M = K = 1$ and $n = 0.8$ are demonstrated in Figures 6 (a) to (c). When $Q > 0$, it characterises heat generation whereas when $Q < 0$, it signifies heat absorption. Figures 6 (a) and 6 (c) display less significant change on velocity and concentration profiles with different values of Q. As heat is generated as Q rises, thus, it leads to enhancement of the fluid temperature as shown in Figure 6 (b). In addition, the region of hot fluid growths at the upper-right cavity, represented by the red region in Figure 7 (b). The data in Table 5 indicates that as Q increases from -1 to 1, the Nu decreases monotonically from 1.4317 to 0.6443, showing a reduced rate of heat transfer at the surface due to diminishing temperature gradients. Conversely, Sh increases consistently from 3.5635 to 4.5982, suggesting an enhanced mass transfer rate at the lid as Q increases. This inverse relationship between Nu and Sh implies a trade-off between thermal and mass transfer dynamics, likely influenced by changes in fluid properties or boundary layer behaviour under varying heat generation/absorption conditions.

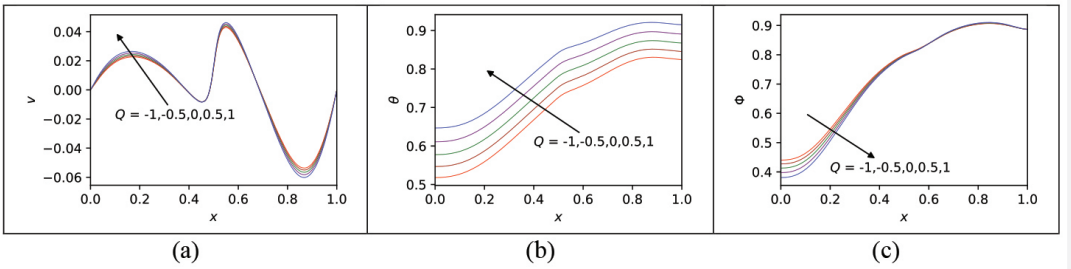

Figure 6: Variation of heat generation/absorption parameter (Q) on (a) velocity, (b) temperature, and (c) concentration profiles at $y = 0.6$

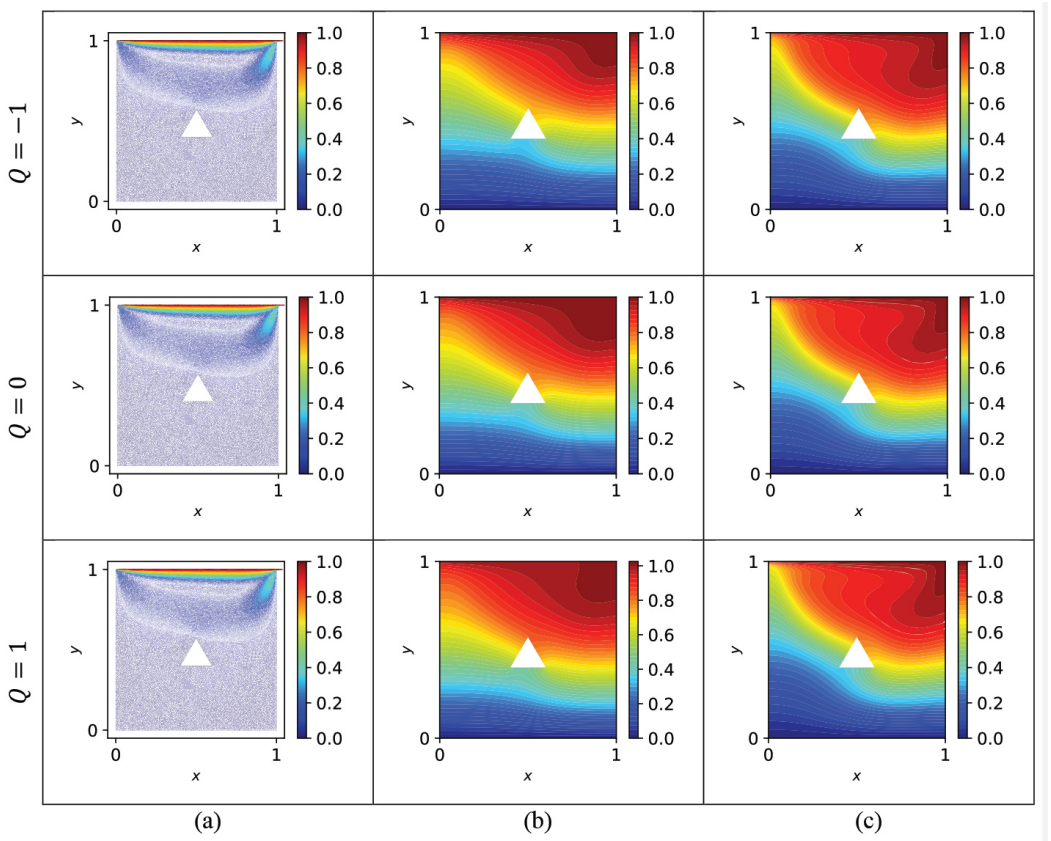

Figure 7: Variation of heat generation/absorption parameter (Q) on (a) velocity, (b) temperature, and (c) concentration profiles in the cavity

Table 5: Comparison of Nusselt number and Sherwood number for $-1 \leq Q \leq 1$

Q	Nusselt Number (Nu)	Sherwood Number (Sh)
-1	1.4316931	3.5634598
-0.5	1.2513337	3.7938124
0	1.0607734	4.0415138
0.5	0.8588705	4.3087814
1	0.6443176	4.5981556

Figures 8 (a) to (c) present the effect of chemical reaction (K) on the vertical v-velocity, temperature, and concentration profiles with $M = Q = 1$ and $n = 0.8$. It is called destructive reaction if $K > 0$ and generative reaction if $K < 0$. Figures 8 (a) and (b) show no significant change as K varies for both velocity and temperature profiles. However, concentration profile shows declining trend as K inclines. As $K > 0$, the process of breaking chemical bond makes the fluid concentration to drop. Different behaviour happens at $K < 0$, where the process of making new chemical bonds increases the fluid concentration as shown in Figure 9. Highly concentrated fluid represented by the red region is detected at the upper side of the cavity, where $K = -1$. The analysis in Table 6 reveals that as K increases, Nu will decrease almost linearly,

indicating a slight reduction in heat transfer efficiency. Conversely, *Sh* increases significantly in a nonlinear trend, suggesting an improvement in mass transfer efficiency with higher reaction rates. For negative values of *K*, *Sh* is lower, likely due to inhibited reaction rates while *Nu* is slightly higher, indicating improved thermal transport. The positive values of *Sh* but reduced values of *Nu* reflects a trade-off between heat and mass transfer influenced by *K*.

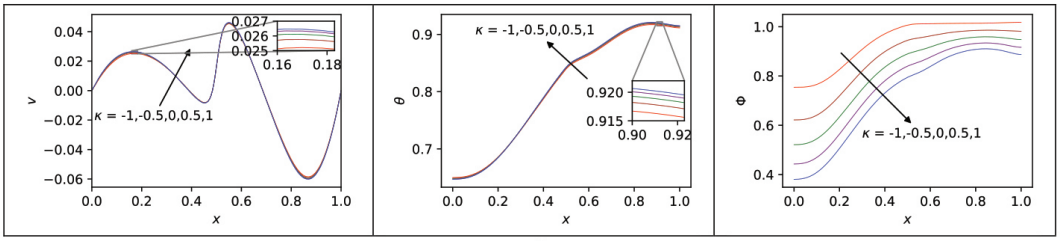

Figure 8: Variation of chemical reaction parameter (*K*) on (a) velocity, (b) temperature, and (c) concentration profiles at $y = 0.6$

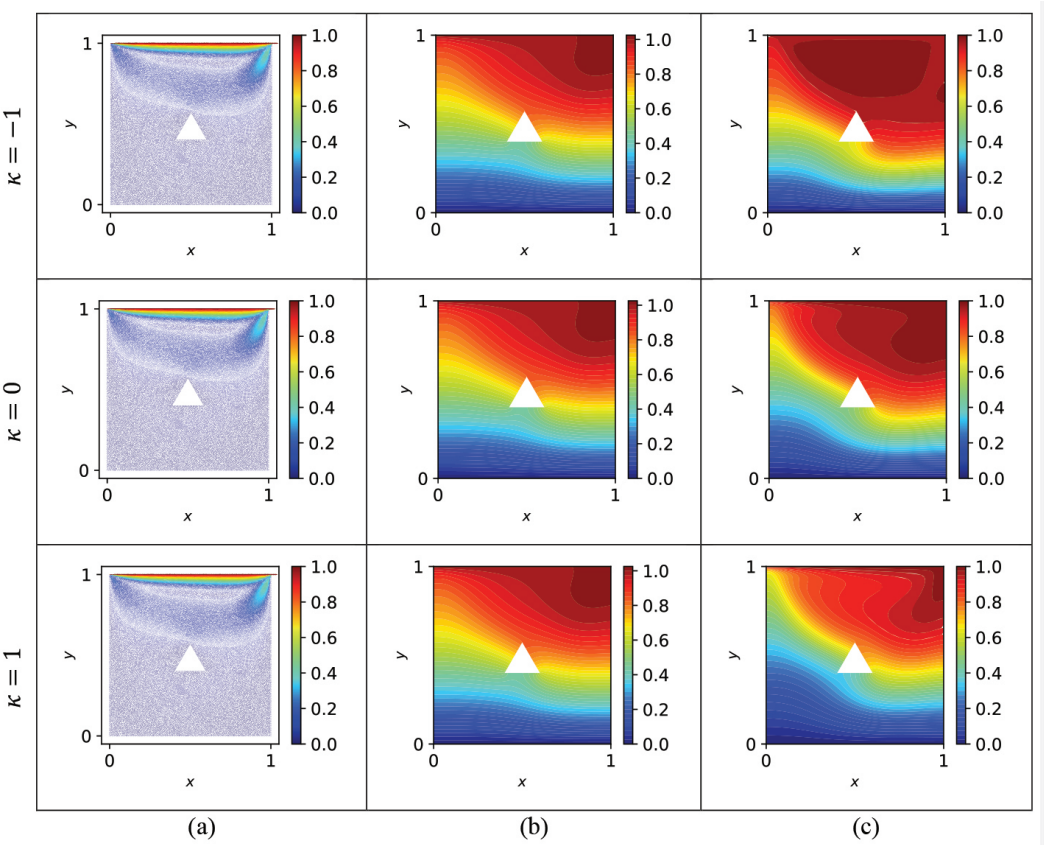

Figure 9: Variation of chemical reaction parameter (*K*) on (a) velocity, (b) temperature, and (c) concentration profiles in the cavity

Table 6: Comparison of Nusselt number and Sherwood number for $-1 \leq K \leq 1$

K	Nusselt Number (Nu)	Sherwood Number (Sh)
-1	0.6591297	-0.5968879
-0.5	0.6543591	0.9842947
0	0.6504176	2.3467300
0.5	0.6471150	3.5399123
1	0.6443176	4.5981556

Conclusions

MHD mixed convective flow of power-law nanofluid in a lid-driven cavity containing solid triangular block with heat generation/absorption and chemical reaction effects is studied. The dimensionless governing equations (6) to (9) with boundary conditions (11) are solved using FEniCS. This automated solution technique offers simple way to solve PDEs directly in vector form. The results show that:

- Increasing power-law index enhances all profiles while increasing magnetic parameter reduces them.
- The temperature profile exhibits an increasing trend due to the influence of the heat generation parameter.
- An increase in the chemical reaction rate has caused a decline in the concentration profile.

Acknowledgements

The authors like to acknowledge the Ministry of Higher Education Malaysia and Research Management Centre, International Islamic University Malaysia (IIUM) for financial support through project ID FRGS/1/2019/STG 06/UIAM/02/3.

Conflict of Interest Statement

The authors declare that they have no conflict of interest.

References

Ahmad, U., Ashraf, M., Abbas, A., Rashad, A. M., & Nabwey, H. A. (2021). Mixed convection flow along a curved surface in the presence of exothermic catalytic chemical reaction. *Scientific Reports*, *11*(1), 12907.

Alhussain, Z. A. (2022). Mixed convective flow in a multiple port ventilation square cavity with insulated baffle. *Case Studies in Thermal Engineering*, *30*, 101785.

Ali, M. M., Akhter, R., & Alim, M. A. (2022). Magneto-mixed convection in a lid driven partially heated cavity equipped with nanofluid and rotating flat plate. *Alexandria Engineering Journal*, *61*(1), 257-278.

Ali, N., Bahman, A. M., Aljuwayhel, N. F., Ebrahim, S. A., Mukherjee, S., & Alsayegh, A. (2021). Carbon-based nanofluids and their advances towards heat transfer applications—A review. *Nanomaterials*, *11*(6).

Alnæs, M., Blechta, J., Hake, J., Johansson, A., Kehlet, B., Logg, A., Richardson, C., Ring, J., Rognes, M., & Wells, G. (2015). *The FEniCS project version 1.5. 3*.

Alsabery, A. I., Armaghani, T., Chamkha, A. J., & Hashim, I. (2020). Two-phase nanofluid model and magnetic field effects on mixed convection in a lid-driven cavity containing heated triangular wall. *Alexandria Engineering Journal*, *59*(1), 129-148.

Bognár, G., Gombkötő, I., & Hriczó, K. (2012). Power-law non-Newtonian fluid flow on an inclined plane. *International Journal of Mathematical Models and Methods in Applied Sciences*, *6*, 72-80.

Buongiorno, J. (2006). Convective transport in nanofluids. *Journal of Heat Transfer*, *128*(3), 240-250.

Chowdhury, K., & Alim, Md. A. (2023). Mixed convection in a double lid-driven wavy shaped cavity filled with nanofluid subject to magnetic field and internal heat source. *Journal of Applied Mathematics*, *2023*, 1-13.

Desai, A. (2022). *Solving stochastic PDEs using FEniCS and UQtk*.

Gangawane, K. M., Oztop, H. F., & Abu-Hamdeh, N. (2018). Mixed convection characteristic in a lid-driven cavity containing heated triangular block: Effect of location and size of block. *International Journal of Heat and Mass Transfer*, *124*, 860-875.

Grzesik, W. (2021). Nanofluid assistance in machining processes- Properties, mechanisms and applications: A review. *Journal of Machine Engineering*, *21*(2), 75-90.

Hafeez, M. B., Amin, R., Nisar, K. S., Jamshed, W., Abdel-Aty, A. -H., & Khashan, M. M. (2021). Heat transfer enhancement through nanofluids with applications in automobile radiator. *Case Studies in Thermal Engineering*, *27*, 101192.

Hossen, S., Imtiaz, Md. N., Hoque, M., Saha, S., & Hasan, M. N. (2019). Analysis of mixed convection heat transfer in a lid-driven partially layered porous square cavity. *AIP Conference Proceedings*, *2121*(1), 070019.

Ismael, M. A., & Chamkha, A. J. (2015). Mixed convection in lid-driven trapezoidal cavities with an aiding or opposing side wall. *Numerical Heat Transfer*, *Part A: Applications*, *68*(3), 312-335.

Ismael, M. A., & Ghalib, H. S. (2018). Double diffusive natural convection in a partially layered cavity with inner solid conductive body. *Scientia Iranica*, *25*(5), 2643-2659. DOI: 10.24200/sci.2017.4349.

Iwatsu, R., Hyun, J. M., & Kuwahara, K. (1993). Mixed convection in a driven cavity with a stable vertical temperature gradient. *International Journal of Heat and Mass Transfer*, *36*(6), 1601-1608.

Kefayati, G. H. R. (2017). Mixed convection of non-Newtonian nanofluid in an enclosure using Buongiorno's mathematical model. *International Journal of Heat and Mass Transfer*, *108*, 1481-1500.

Keya, S. T., Yeasmin, S., Rahman, M. M., Karim, M. F., & Amin, M. R. (2022). Mixed convection heat transfer in a lid-driven enclosure with a double-pipe heat exchanger. *International Journal of Thermofluids*, *13*, 100131.

Khan, N. S. (2019). Mixed convection in MHD second grade nanofluid flow through a porous medium containing nanoparticles and Gyrotactic microorganisms with chemical reaction. *Filomat*, *33*(14), 4627-4653.

Kumar, S., Gangawane, K. M., & Oztop, H. F. (2021). A numerical study of mixed convection in a two-sided lid-driven tall cavity containing a heated triangular block for non-Newtonian power-law fluids. *Heat Transfer*, *50*(5), 4806-4829.

Logg, A., Wells, G., & Mardal, K. -A. (2011). Automated solution of differential equations by the Finite Element Method: The FEniCS book. In *Lecture notes in computational science and engineering* (Vol. 84).

Nouari, S., EIHamdani, S., Bendou, A., & Bara, E. (2021). Three-dimensional numerical simulation of mixed convection of nanofluid inside a double lid-driven differentially heated cavity. *AIP Conference Proceedings*, *2345*(1), 020005.

Owhaib, W., & Al-Kouz, W. (2022). Three-dimensional numerical analysis of flow and heat transfer of bi-directional stretched nanofluid film exposed to an exponential heat generation using modified Buongiorno model. *Scientific Reports*, *12*(1), 10060.

Rashidi, M. M., Sadri, M., & Sheremet, M. A. (2021). Numerical simulation of hybrid nanofluid mixed convection in a lid-driven square cavity with magnetic field using high-order compact scheme. *Nanomaterials*, *11*(9).

Reddy, N. N., Rao, V. S., & Reddy, B. R. (2021). Chemical reaction impact on MHD natural convection flow through porous medium past an exponentially stretching sheet in presence of heat source/sink and viscous dissipation. *Case Studies in Thermal Engineering*, *25*, 100879.

Scott, T. O., Ewim, D. R. E., & Eloka-Eboka, A. C. (2022). Hybrid nanofluids flow and heat transfer in cavities: A technological review. *International Journal of Low-carbon Technologies*, *17*, 1104-1123. https://doi.org/10.1093/ijlct/ctac093

Selimefendigil, F., & Chamkha, A. J. (2019). Magnetohydrodynamics mixed convection in a power law nanofluid-filled triangular cavity with an opening using Tiwari and Das' nanofluid model. *Journal of Thermal Analysis and Calorimetry*, *135*(1), 419-436.

Thohura, S., Molla, Md. M., Sarker, M. M. A., & Paul, M. C. (2021). Study of mixed convection flow of power-law fluids in a skewed lid-driven cavity. *Heat Transfer*, *50*(6), 6328-6357.

Tiwari, R. K., & Das, M. K. (2007). Heat transfer augmentation in a two-sided lid-driven differentially heated square cavity utilising nanofluids. *International Journal of Heat and Mass Transfer*, *50*(9), 2002-2018.

Zhang, L. (2021). Chapter 9 - Application of fractal theory in transient pressure properties of hydrocarbon reservoir. In Cai, J., Zhang, L., & Wei, W. (Eds.), *Modelling of flow and transport in fractal porous media* (pp. 193-249). Elsevier.